Available online at www.sciencedirect.com

ScienceDirect

Procedia Materials Science 8 (2015) 868 – 877

Procedia Materials Science

www.elsevier.com/locate/procedia

International Congress of Science and Technology of Metallurgy and Materials, SAM - CONAMET 2013

Effect of the tool penetration depth in Friction Stir Spot Welding (FSSW) of dissimilar aluminum alloys

Joaquín M. Piccini[a,b], Hernán G. Svoboda[b,c]*

[a]*PSA Peugeot Citroen Argentina, Peron 1001, Villa Bosch B1683BXN, Argentina*
[b]*Welding Technology and Mechanical Behavior of Metallic Materials Group, INTECIN, School of Engineering, University of Buenos Aires, Ciudad de Buenos Aires 1127, Argentina*
[c]*Consejo Nacional de Investigaciones Científicas y Técnicas (CONICET), Ciudad de Buenos Aires C1033AAJ, Argentina*

Abstract

In the last years Friction Stir Welding has produced a big impact on several industries due to its advantages. Particularly, automotive industry has developed a variant of the original process named Friction Stir Spot Welding (FSSW), having a strong influence on welding of thin sheets of aluminum alloys and dissimilar materials. Nevertheless, the knowledge about the influence of welding procedure on joint characteristics is scarce, mainly for dissimilar materials. The aim of this work was to study the effect of the tool penetration depth during welding, as well as, the relative position of the materials used in the superimposed joints, when AA5052-AA6063 sheets samples were welded. Tool penetration depths between 0.05 and 1.25 mm were analyzed, for both materials positions. Macrostructural and dimension characterization, microhardness profiles and Peel tests (PT) were done for different conditions. The fracture loads in PT increased with the tool penetration depth for both material positions, being higher when AA6063 was the upper material. However, the tool penetration depth has a limit in the increasing of fracture load, for which the fracture mechanism changes from interfacial to circumferential.

© 2015 The Authors. Published by Elsevier Ltd. This is an open access article under the CC BY-NC-ND license (http://creativecommons.org/licenses/by-nc-nd/4.0/).
Selection and peer-review under responsibility of the scientific committee of SAM - CONAMET 2013

Keywords: Friction Stir Spot Welding; Aluminum; Dissimilar; Peel Test.

* Corresponding author. Tel.: +54-11-4514-3009; fax: +54-11-4514-3010.
E-mail address: hsvobod@fi.uba.ar

2211-8128 © 2015 The Authors. Published by Elsevier Ltd. This is an open access article under the CC BY-NC-ND license (http://creativecommons.org/licenses/by-nc-nd/4.0/).
Selection and peer-review under responsibility of the scientific committee of SAM - CONAMET 2013
doi:10.1016/j.mspro.2015.04.147

1. Introduction

In the last years, a critical trend in automotive manufacturing has been the increasing use of lightweight alloys in replacement of traditional steels. The use of aluminum alloys for auto body panels leads to a reduction in the vehicle weight which reflects on reduced emissions and an increased performance. After the body panels are formed into the desired shapes, they will require joining to other parts of the automobile. Current closure panel welding techniques include RSW, SPR, and clinching. The disadvantages of these methods include weld electrode dressing, high energy consumption and the use of consumables. In the case of RSW, higher electric power source and electrode dresser are required because of the physical properties of the aluminum alloy. Also, the level of defects in the welded area is higher than in the welding of steel sheets (Mishra and Mahoney (2007), Wang and Lee (2006), Kou (2003)). The SPR also requires rivets that add to the cost of assembly manufacturing via consumables. The welding method used for aluminum sheet assembly is one of the key technology drivers to enhance weight reduction in the automotive industry. The FSSW technique was invented by Mazda and has been evaluated as an alternative welding technique. This technology was first used in the Mazda RX-8 rear door panel spot welding in 2003, claiming to have reduced the energy consumption by 99% of that used by the conventional earlier process. During this process, a rotating tool with a probe is plunged into the material from the top surface for a certain period of time to generate frictional heat. At the same time, a backing plate contacts the lower sheet from the bottom side to support the downward force. Heated and softened material adjacent to the tool causes plastic flow. In addition, the tool shoulder gives a strong compressive force to the material. After the tool is drawn away from the material, a solid-phase weld is produced between the upper and the lower sheets. Figure 1 shows the appearance and the cross-sectional configuration of a FSSW joint (Mishra and Mahoney (2007)).

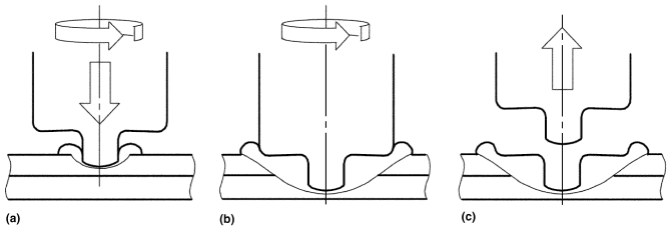

Fig. 1. (a) Plunging; (b) Bonding; (c) Drawing out.

The total heat input that the base materials receive is lower than any traditional fusion welding technique, were the base materials are melted. Furthermore, the size of the HAZ is smaller and so are the residuals stresses and the distortions of the welded sheets. Moreover, the microstructural changes related to the thermal cycle of the welding are reduced. This is especially important in heat treatable aluminum alloys (ASM Handbook (1990)).

The key issue to resolve is the relationships between process parameters, material flow, resulting microstructure and the subsequent strength and failure mode of welded joints. Properly welded joints will have high shear strength and will fail by “tear-out” of a large section of the joined interface. Conversely, poorly welded joints will fail in a brittle manner at the weld nugget (Tozaki et al. (2007)). In the last years, dissimilar welding has reached a strong relevance in welding technology, especially in automotive industry. FSSW is a process particularly appropriated for those applications. Nevertheless, there are a lot of aspects of dissimilar FSSW that still requires further research.

Several process features may play a critical role in determining joint integrity. These include, but are not limited to, tool geometry, tool rotational speed, holding time, tool downwards force, tool penetration depth, sheet surface preparation and post weld heat treatment. It has been previously suggested that these mentioned aspects have an important effect on joint properties, particularly the tool penetration depth (TPD) (Francesco and Svoboda (2013)). The variation of the TPD changes the depth which the rotating tool shoulder presses onto the top sheet, affecting the resulting microstructure of that region.

The objective of this study was to analyze the influence of the tool penetration depth, as well as the relative position of the dissimilar aluminum alloys (AA5052-H32/AA6063-T6) in superimposed joints, on the spot conformation and mechanical properties of FSSW welded joints.

Nomenclature

RSW	Resistance Spot Welding
SPR	Self-Piercing Rivets
FSW	Friction Stir Welding
FSSW	Friction Stir Spot Welding
TPD	Tool Penetration Depth
M	Macrographic Sample
P	Peel Test Sample
PS	Tool Plunge Speed
RS	Tool Rotational Speed
HAZ	Heat Affected Zone
TMAZ	Termomechanical Affected Zone
SZ	Stir Zone
BM	Base Material
SLM	Stereo Light Microscopy
H	Indentation height measured on the macroscopic images
Kr	Hook Height
A	Effective welded width
K	Minimum Hook Height
P	Remaining thickness of the lower plate
Dh	Shoulder Diameter
IH	Minimum distance between the interface and the shoulder surface
PT	Peel Test
Fl	Fracture Load

2. Experimental Procedure

Dissimilar welds, with different relative position of the aluminum alloys were produced with the TPD varying from 0.05 to 1.25 mm. The materials used were aluminum 5052-H32 and 6063-T6 sheets, with thicknesses of 3 mm and 2 mm, respectively. The tool used for FSSW was made of tool steel (H13) with a Dh of 12 mm and a concave profile. The pin was conical unthreaded, with 3.8 mm in length and 3.5 mm of end diameter. All the friction stir welds were made with a RS of 680 RPM, a PS of 19 mm/s and a dwell time of 2 s. Figure 2a shows the clamping device used. For each condition two types of samples were welded. One was used to do the macrostructural and dimensional analysis, as well as the microhardness profile (M sample, figure 2b). The other one was used for Peel Tests (P sample, figure 2c).

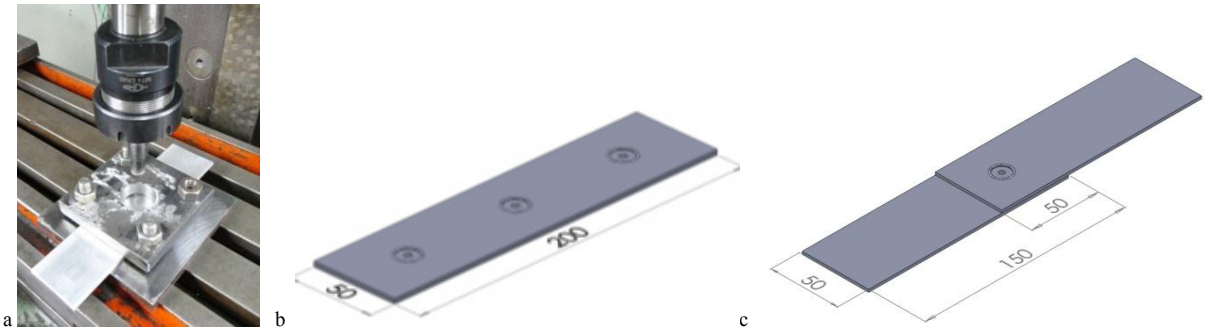

Fig. 2. (a) Clamping device; (b) M sample; (c) P sample.

Table 1 lists the analysed welding conditions and the identification used for each sample. The samples names include the sheets relative position and the TPD.

Table 1. Main welding parameters and sample identification.

Sample	Top Sheet material	Sample type	TPD (mm)
5-6-05	5052	P	0,05
5-6-2	5052	P, M	0,2
5-6-6	5052	P, M	0,6
5-6-10	5052	P, M	1,0
5-6-12	5052	P, M	1,25
6-5-2	6063	P, M	0,2
6-5-4	6063	P	0,4
6-5-7	6063	P, M	0,7
6-5-10	6063	P, M	1,0
6-5-12	6063	P, M	1,25

The specimens for metallographic examination were sectioned to the required sizes comprising the SZ, TMAZ, HAZ and BM regions. After metallographic preparation the specimens were etched with the Keller's reagent to reveal their microstructures (ASM Handbook Volume 09 (2004)). Metallographic observations were done using SLM. Figure 3 shows a schematic plot of a cross section of the welded spot where the dimensions measured are indicated.

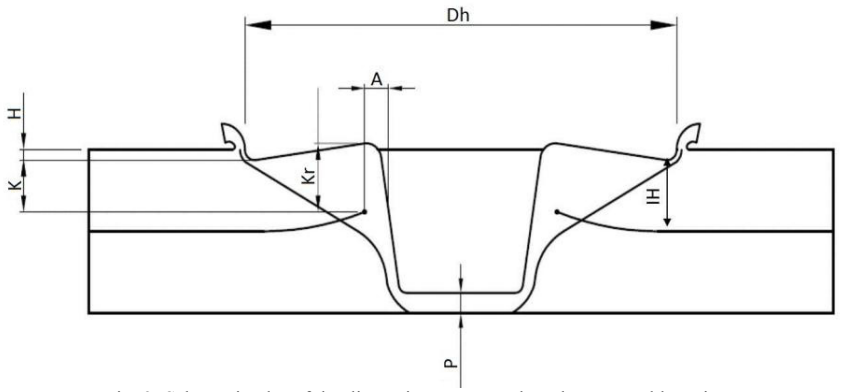

Fig. 3. Schematic plot of the dimensions measured on the spot weld sections.

Kr is defined as the distance between the beginning of the metallurgical bond and the upper sheet surface. A is defined as the distance between the pin surface and the beginning of the metallurgical bond. H is the distance between the upper sheet surface and the lower point reached by the shoulder. The reduced thickness of the central part of the nugget, due to the tool probe penetration at the bottom of the central hole, is P. The minimum thickness of the upper sheet, inside the SZ, is denoted as K. Finally, IH is the distance between the lower position of the shoulder surface and the interface between both sheets.

Mechanical properties of the spots welded were characterized using microhardness profile and Peel tests. Vickers microhardness profile was obtained by measuring along an horizontal line at the hook height, with a load of 0.1 kg and a loading time of 10 seconds, according to ASTM E384 standard. The Peel test was performed using an Instron TT10-DM universal testing machine at a constant cross-head speed of 1 mm/min. Load and displacement were recorded, obtaining the load-displacement curves. The Fl was obtained for each condition. Finally, fracture surfaces were observed by SLM.

3. Results and Discussion

3.1. Materials

The AA5052 aluminum alloy includes Mg (0.41wt%) as main alloy element, some content of Fe (0.38wt%) and traces of Si (0.09wt%), Cr (0.02wt% and Mn (0.02wt%). The H32 condition describes the cold strain hardening that this material experienced. The microhardness of the AA5052-H32 was 70 HV. The AA6063 contains Mg (0.41 wt%), Si (0.41 wt%), Cu (0.81 wt%), Fe (0.85 wt%), Zn (0.52 wt%) and Mn (0.11 wt%). Traces of Ni (0.02 wt%), Cr (0.02 wt%) and Pb (0.02 wt%) were also measured. This alloy is considered as heat treatable, and it was on T6 condition. The AA6063 microhardness was 90 HV.

3.2. Welds surface appearance

Figures 4a to 4d show several friction stir spot welds achieved with different TPD and sheet position. An excellent appearance can be observed in the welded spots for all the welding conditions studied. Welding parameters, such as the TPD, affect the heat generation and the material flow. The 5-6-05 sample (Fig. 4a) shows the lowest penetration depth, while the 6-5-12 sample (figure 4d) has the highest TPD. The material of the top surface is squeezed out and accumulated along the outer circumference of the shoulder indentation. Finally, it can be observed that the material flow out of the spot increases with tool penetration depth.

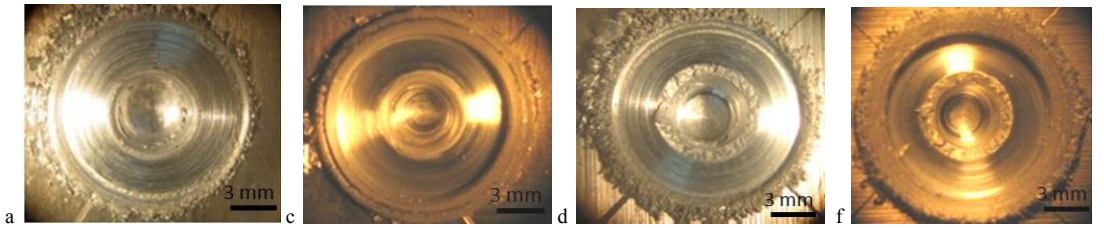

Fig. 4. Welds surface appearance. (a) 5-6-05; (c) 5-6-6; (d) 6-5-2; (f) 6-5-12.

3.3. Macrostructure and dimensional characterization

Macrographic observations along the symmetry plane of the spot welds cross sections, obtained with different welding conditions, are shown in figures 5a to 5f. The indentation profile reveals the general shape of the probe and the concave shoulder of the welding tool, showing a good material flow, like it was observed by Yang et al. (2010). For all welding conditions studied, the joints are defects free, as shown in figures 5a to 5f.

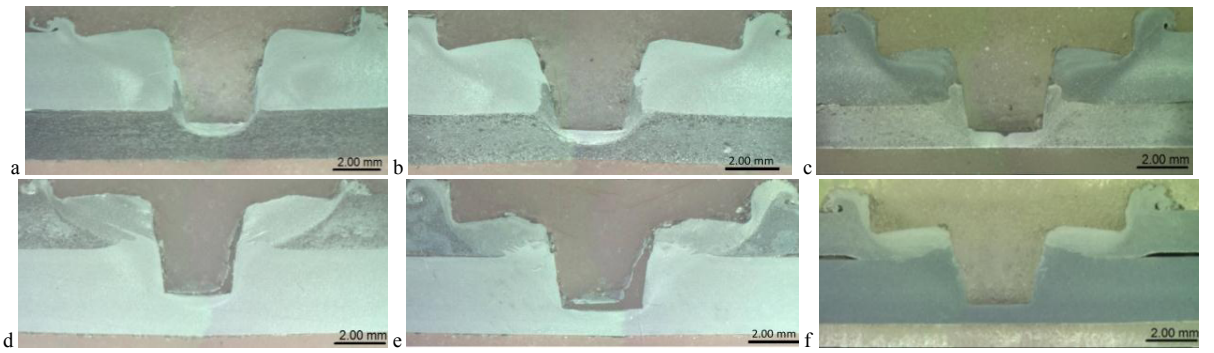

Fig. 5. Macrographic appearance of the welded joints: (a) 5-6-2; (b) 5-6-6; (c) 5-6-10; (d) 6-5-2; (e) 6-5-7; (f) 6-5-10.

The plastic flow observed is related with the frictional heat due to the plunging action of the rotational tool. A circular protrusion forms on the upper sheet. Due to high pressure and large plastic deformation, the upper and lower

sheets are compressed together to form and effective joint in the vicinity of the probe (Yang et al. (2010), Tran et al. (2009)). An area near the central hole of the pin and the shoulder contact is observed, which has fine grains and it is called SZ. As shown in figures 5a to 5f, a layer of the lower sheet material that was pushed and deformed by the tool pin, can be seen mixed with the material of the upper sheet, near the central hole. Due to the rotating pin penetration, the heated and softened upper sheet material was pushed down near the probe. Also, heated and softened lower sheet material rose upward and outward due to the probe penetration. As the TPD increases, the flow of the lower sheet material into the upper one increases, as was also found by Tran et al. (2009). Note that for the higher tool shoulder indentation, a radial expansion of the upper sheet material along the outer circumference of the tool shoulder indentation was produced. Due to the constraint of the neighboring material, the upper sheet was therefore slightly bent along the outer circumference of the tool shoulder indentation.

According to the microscopic characteristics of the cross-section, four regions can be identified: SZ, TMAZ, HAZ and the BM. The BM is remote from the weld and it has not been deformed nor heat affected, as seen in figure 6d. Compared with BM, the HAZ (figure 6c) is closer to the weld center and the material in this region has experienced a thermal cycle that modified its structure and mechanical properties. The TMAZ exhibits deformed grains, and a fraction of precipitates are oriented according the material flow as is shown in figure 6b. Dynamic recrystallization occurred in the periphery of the probe and under the shoulder producing the SZ (figure 6a), which is characterized by refined and equiaxed grains. In this zone, precipitates are broken into particles and dissolved by the stirring of the tool (Mishra and Mahoney et al. (2007)). Two interface tips can be seen in the cross section that represent the end of the welded zone, which are named “hook”.

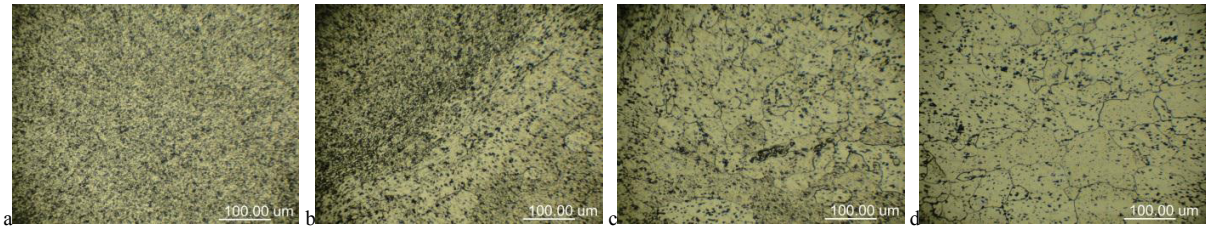

Fig. 6. Micrographic appearance a welded joint: Sample 6-5-2. (a) SZ; (b) TMAZ; (c) HAZ; (d) BM.

The hook refers to the last visible point of the interface between both sheets into the SZ, becoming a geometrical defect that affects the integrity of spot welds because cracks can propagate along it when the weld is subjected to external loading (Tran et al. (2009)). The hook spreads upward up to reach a final position in the upper sheet stir zone, exhibiting a jagged form as figure 7 shows. During welding, the hook is formed because of the upward material flow of the sheets interface, caused by the penetration of the tool (Yang et al. (2010)). Furthermore, the oxide film on the sheets interfaces is broken up into particles by stirring of the tool and could be dispersed into the weld region, which can affect the metallurgical bonding. Although no defect can be seen on the cross section of the welds, figures 5a to 5f show several differences on the macrostructure of the joints when the TPD and the position of the alloys are changed. Moreover, the increase of the TPD implies more material flow in the interface of the joint, locating the final hook position far away from the sheets interface and from the keyhole surface, as was also observed by Yang et al. (2010). This phenomenon was maximized for 6-5 configuration. In this sense, figures 5a to 5f show that for the same indentation, the upward flow is higher in the 6-5 configuration than in the 5-6.

In FSSW, heat is generated by friction and plastic deformation, which is influenced by the weld parameters, thermal conductivities of the workpiece, weld tool geometry and backing anvil. Early experimental studies showed that the majority of the heat generation occurs at the shoulder/workpiece interface (Mishra and Mahoney (2007)). The established material flow is related with the generated heat and material properties. Figure 7, shows the microstructural appearance of the welded joint in the SZ, particularly at the interface zone, showing the final position of the hook of 6-5-2 and 5-6-2 samples. Moreover, it shows the effective plastic flow and the interaction between the two welded materials. The interface becomes diffuse until it finally disappears, producing the metallurgical joint. It must be pointed out the difference in the length of A in both cases. For the 6-5 configuration, A is larger than for the 5-6 configuration, although the TPD is the same for both spots.

a b

Fig. 7. Final position and appearance of the hook: (a) 6-5-2; (b) 5-6-2.

Despite the TPD used is the same for both samples, as the thicknesses of both plates is not the same, the final distance between the shoulders surface and the interface (IH) is different. That is why IH measures how much of the heat input arrives to the interface, without considering the relative thicknesses.

In order to analyze the evolution of the welded joint with the process parameters, the dimensions shown in figure 3 were measured. These characteristic weld dimensions depend on the welding parameters and define the effective bonded areas, so they would be related with the mechanical properties of the joint, for different welding conditions (Wang and Lee (2006), Francesco and Svoboda (2013)). The results are shown in table 2.

Table 2. Dimensions of the FSSW joints.

Sample	H (mm)	P (mm)	Dh (mm)	A (mm)	Kr (mm)	K (mm)	IH (mm)
5-6-2	0,19	1,49	11,98	0,35	3,19	2,85	3,06
5-6-6	0,6	1,19	12,01	0,58	2,97	2,48	2,70
5-6-10	1,02	0,94	11,71	0,68	2,14	1,96	2,36
5-6-12	1,07	0,86	11,60	0,71	1,95	1,61	2,29
6-5-2	0,17	1,5	11,38	1,4	1,71	1,54	1,93
6-5-7	0,83	1,03	12,05	1,91	1,39	1,09	1,31
6-5-10	0,99	0,89	11,52	1,77	1,20	0,92	1,24
6-5-12	1,09	0,82	11,61	2,07	1,03	0,69	1,14

It was observed that TPD has an influence on the different characteristic dimensions of the welded joint, as well as the relative position the aluminum sheets. As a general trend A increased with the TPD, while P, K, Kr and IH decreased, as shown in table 2. Figure 8a shows the effect of real indentation (H) on the effective weld width (A), for both configurations. The effective weld width (A) increases linearly with the tool penetration depth, for both configurations. This is due to the higher effect of the tool shoulder on heat and material flow when it gets closer to the interface. However, there is a large difference in A with the relative position of the aluminum alloys.

For 6-5 configuration A is larger than for 5-6. This is related to two superimposed effects. AA5052 alloy can be more easily deformed than the AA6063 alloy; consequently the material flow is higher when the AA5052 alloy is in the lower position, resulting in a hook position far away from the pin hole. Additionally, the difference seen in figure 8a is also related to the relative thicknesses of both sheets. AA6063 alloy sheet was 2 mm thick while the AA5052 alloy was 3 mm thick. When the AA5052 sheet is in the upper position, a given indentation produces lower material flow at the interface than in the opposite configuration because of the tool shoulder-sheets interface is larger for this configuration, producing less thermomechanical effect on the mentioned interface. Therefore IH is a parameter that takes into account the effect of the tool shoulder on the interface in a better way, particularly when dissimilar thicknesses are compared.

In order to analyze the strength of the welded joints, other dimensions related to the effective remnant thickness are also important: Kr, K, IH. Figure 8b shows the effect of TPD on Kr, for both configurations. Kr decreases as H increases. This observation could be related to the relative position of the shoulder respect to the interface, which decreases with H. Indeed, a deeper indentation produces greater flow near the interface, generating a higher height of the hook, explaining the non-linear variation observed. As was mentioned above, the 6-5 configuration produces a higher upwards flow of AA5052 into AA6063 upper sheet, achieving smaller Kr values. These values will affect the mechanical properties of the joints. In Peel tests, A is going to be the resistance section to the interfacial failure mode, while Kr, K or IH are going to be related with the resistance section for tear out failure mode. According to

this, both dimensions must be optimized to achieve a balance between them to maximize the fracture loads in Peel tests.

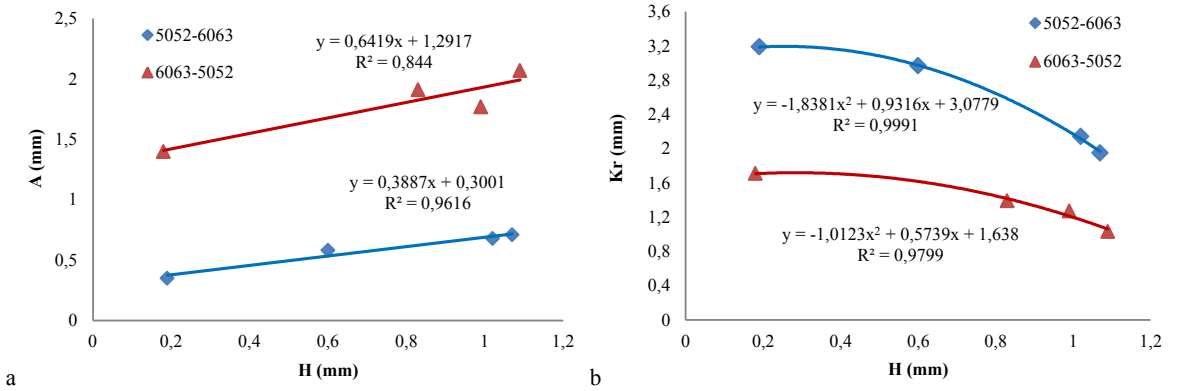

Fig. 8. Effect of indentation (H) on: (a) Effective welded width (A) and (b) hook height (Kr), for both configurations.

3.4. Microhardness

The AA6063-T6 is a heat treatable alloy strengthened by precipitation of second phases coherent with the matrix. AA5052-H32 is strengthened by work hardening (Mishra and Mahoney (2007), Kou (2003)). The microhardness evolution in the surroundings of the welded zone will be different, depending on the alloy being in the upper position. Figure 9 shows the microhardness profiles, measured at the hook height (yellow line) obtained for a sample of both configurations. These results are representative of those obtained for all the welded conditions studied.

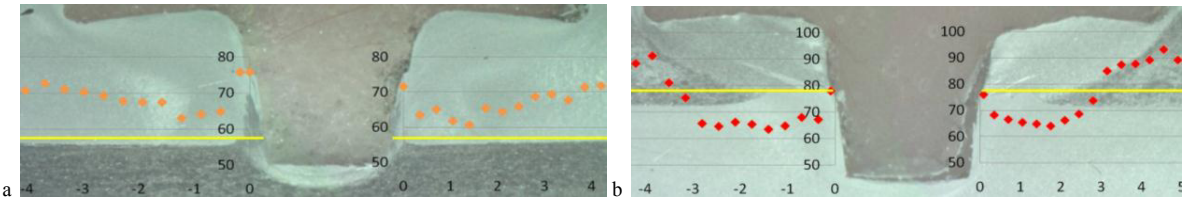

Fig. 9. Microhardness profiles: (a) 5-6-2; (b). 6-5-2.

For 5-6 configuration (figure 9a) there is a slight decrease in hardness from the base metal (70 HV) towards the pin hole (60 HV) in the HAZ. This effect can be attributed to some degree of recrystallization during FSSW, producing a softening of the microstructure. In the SZ, the recrystallization and grain refinement are so intense that produce an increase in the hardness. Next to de pin surface a mixture of both materials is observed, reaching the maximum hardness values (80 HV).

Figure 9b, shows the microhardness evolution of a 6-5 sample. Hardness decreases from the base material (90 HV) towards the HAZ (62 HV) and remains almost unchanged through the SZ. Finally a slightly increase near the pin surface (78 HV) was observed. The hardness evolution is caused by microstructural modifications associated with the elevated temperatures experienced in this zone. For heat treatable aluminum alloys, in the HAZ dissolution of precipitates and/or overaging could take place because of the temperature achieved in this zone during FSSW. The minimum value detected in the HAZ is related with these phenomena. The final hardness increase can be explained by two effects. First, plastic deformation in the TMAZ increased the hardness. Moreover, in the SZ dynamic recrystallization and grain refinement occurs. Finally, near the pin surface a mixture of both materials is observed in accordance with the maximum hardness value in the SZ. Natural aging could take place (Mishra and Mahoney (2007)), because of that, microhardness tests must be related with the period of time elapsed from the welding.

3.5. Peel Tests

Figure 10a shows the fracture loads (Fl) of the welded spots in the Peel Tests as function of H, for both configurations. The fracture load increases with H for both configurations. These results are in accordance with figure 8, where it has been shown that A increases with H, improving the load capacity of the spots when the TPD increases. It has been noted that in 6-5 configuration for the highest value of H, the Fl diminished. The 5-6 configuration does not show a maximum Fl, while the 6-5 configuration reaches the maximum of Fl (5500N) for H = 1 mm.

Figure 10a shows a large difference in the Fl evolution for both configurations. It is clear that the 6-5 configuration presents higher loads for all the indentation (H). This effect is related with the relative thicknesses of both sheets. As discussed above, IH seems to be a more effective value for considering the heat effect of the shoulder on the interface, when comparing both configurations. Figure 10b shows the evolution of the fracture load with IH.

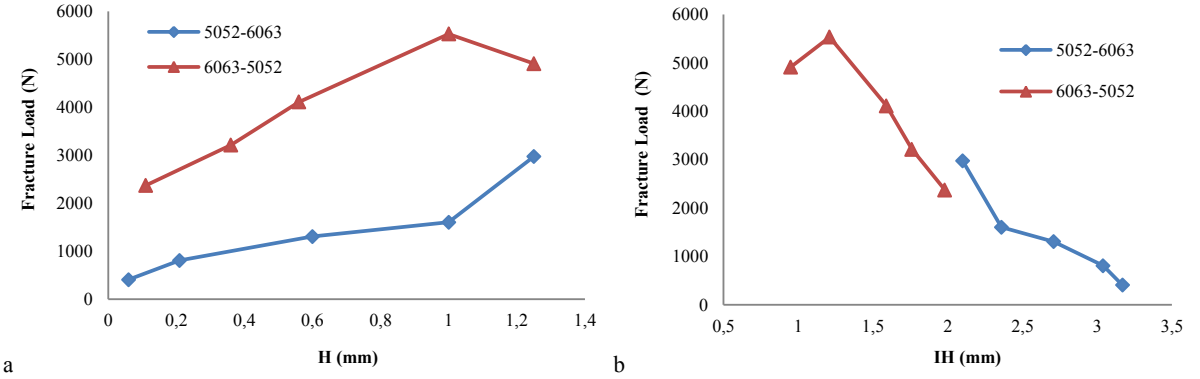

Fig. 10. (a) Effect of indentation (H) and (b) interface distance (IH) on Fracture load (Fl), for both configurations.

As IH decreases the tools shoulder is closer to the sheets interface, increasing the termomechanical effect on it. It can be noted that Fl increases with the reduction of IH. However, there is a limit for this increase in Fl. If IH is too small the fracture load decreases. In coincidence with that drop in fracture load, the fracture mode changes. While the Fl increases with H, the fracture mode was interfacial for both configurations, as shown in figures 11a to 11d.

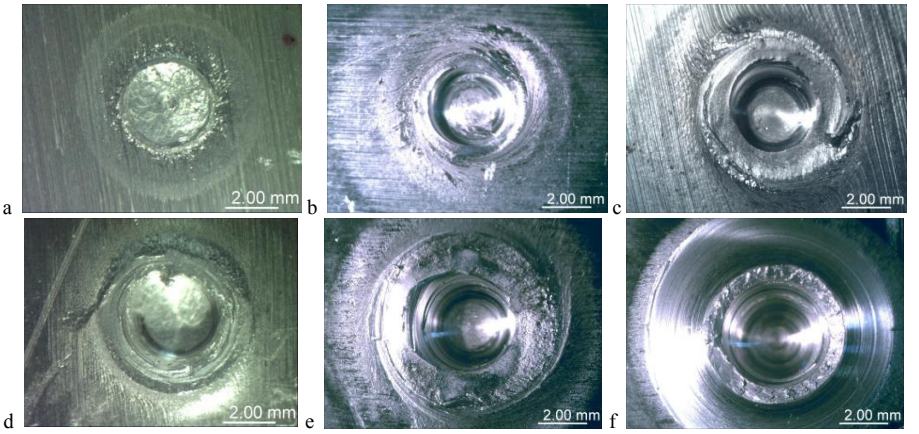

Fig. 11. Fracture surfaces from Peel Tests: (a) 5-6-05; (b) 5-6-6; (c) 5-6-12; (d) 6-5-1; (e) 6-5-10; (f) 6-5-12.

Sample 6-5-10 shows another fracture mode. This sample breaks in a mixed fracture mode (figure 11e), achieving the maximum fracture load (5500 N). For indentations deeper than 1 mm, IH becomes too thin. So, the

fracture load decreases and a circumferential fracture mode was observed (figure 11f).

A proper balance between A and IH leads to the maximum failure load. Tran al. (2009) reported that interfacial fracture modes have lower Fl than tear out fracture modes. Nevertheless, the authors also pointed out that the maximum failure loads are achieved when the completely circumferential fracture mode is obtained. It could be possible to find a higher Fl value for an indentation between 1 and 1.25 mm. The maximum fracture load obtained in Peel tests are higher than those previously reported for these alloys (Tran et al (2009)). The mixed fracture mode is observed (figure 11e) for the maximum Fl. This shows the importance that the TPD and the relative position of the dissimilar sheets (thickness and material) have on the mechanical properties of the joints. An optimum balance between A and IH will maximize the strength of the welded joints when the TPD is increased. For the 6-5 configuration, the value that optimizes this balance is H = 1 mm. In the case of 5-6 configuration that optimum was not reached, being the fracture mode interfacial for all analyzed H values, showing a monotonic increasing of the Fl with H.

4. Conclusions

Friction stir spot welds on dissimilar (materials and thicknesses) aluminium alloys were produced with different TPD and sheets relative position. The joints obtained were sound and defects-free for all the analyzed welding conditions. The plastic flow is affective by the TPD and the relative position of the sheets employed.

The hook final position is related to the plastic flow of the materials involved, defining the effective bonded area, that can be characterized by measuring A and Kr. A increases with the TPD, whereas Kr decreases.

When welding with the AA6063 alloy as the upper sheets (6-5 samples), A was increased when the TPD increases as well as Kr diminished. On the other hand, when AA5052 alloy was in the upper position (5-6 samples), A was lower than for the 6-5 and Kr higher, but both show the same tendency with TPD than in the previous configuration. This is related with the effective action of the tools shoulder on the interface taking into account the tool penetration depth and the relative thicknesses of the sheets employed.

To evaluate the thermomecanical effect of tool shoulder on the interface for dissimilar thicknesses IH is a more effective parameter.

For all analyzed conditions microhardness diminishes from BM towards SZ, reaching the minimum value in the HAZ, for both configurations. In the material located next to the pin surface the microhardness rose. The TPD has not affected the microhardness profiles.

The Fl in the Peel Tests increases with the TPD up to reaching e maximum value associated with the change in the fracture mode. The highest value obtained for the 5-6 configuration was 3000 N with an indentation of 1.25 mm, while it was 5500 N for the 6-5 configuration with a TPD of 1 mm. This limit value is related to a balance between A and IH which is reduced as H increases. The failure mode for the highest Fl was mixed, while it was tear out when the TPD was even higher than 1 mm (in 6-5 configuration). For lower values of H the fracture mode is interfacial.

References

Mishra, R., Mahoney, M., 2007. Friction Stir Welding and Processing. ASM International.

Wang, D., Lee, S., 2006. Microstructures and failure mechanisms of friction stir spot welds of aluminium 6061-T6 sheets. Journal of Materials Processing Technology 186, 291–297.

Kou, S., 2003. Welding Metallurgy. Wiley Interscience.

ASM Handbook Volume 06, 1990. Welding Brazing and Soldering. ASM International.

Tozaki, Y., Uematsu, Y., Tokaji, K., 2007. Effect of tool geometry on microstructure and static strength in friction stir spot welded aluminium alloys. International Journal of Machine Tools & Manufacture 47, 2230–2236.

Francesco, L., Svoboda, H., 2013. Efecto de las variables de proceso de Soldadura de Punto por Fricción Agitación (FSSW) de aluminio en las propiedades mecánicas: Trabajo Profesional de Ingeniería Mecánica. FIUBA.

ASM Handbook Volume 09, 2004. Metallography and Microstructures. ASM International.

Yang, Q., Mironov, S., Sato, Y., Okamoto, K., 2010. Material flow during friction stir spot welding. Materials Science and Engineering A 527, 4389–4398.

Tran, V., Pan, J., Pan, T., 2009. Effects of processing time on strengths and failure modes of dissimilar spot friction welds between aluminium 5754-O and 7075-T6 sheets. Journal of Materials Processing Technology 209, 3724–3739.